Control of unstable steady states in semiconductor lasers by time-delayed feedback methods

Thomas Dahms, Philipp Hövel, Eckehard Schöll

***Abstract*— Time-delayed feedback methods can be used to control unstable periodic orbits as well as unstable steady states. We present an application of extended time delay autosynchronization introduced by Socolar et al. to a semiconductor laser system with undamped relaxation oscillations implemented as a model of Lang-Kobayashi-type. We show that the control method is able to enhance the local stability of the lasing fixed point leading to cw-operation by suppression of unwanted intensity pulsations. Due to the self-feedback, multistable behavior can also occur in the form of delay-induced limit cycles and fixed points for certain choices of the control parameters.**

I. Introduction

Control of chaos has been studied intensely since almost 2 decades [1]. Starting with the work of Ott, Grebogi, and Yorke [2], a variety of control schemes has been invented, which include the *time-delay autosynchronisation* (TDAS), introduced by Pyragas [3]. In TDAS, the control is generated by measuring a system's variable and comparing it to its counterpart some time units τ ago. A control force is then generated from the difference of these values. One groundbreaking advantage of TDAS is the noninvasiveness of the control, meaning that the control force vanishes on the desired orbit. This control scheme was advanced by Socolar et al., leading to the *extended time-delay autosynchronisation* (ETDAS) [4]. In ETDAS, a memory parameter was introduced, which weights earlier states of the system in the control. This was invented in the context of optical systems like semiconductor lasers, where feedback can be realized by Fabry-Perot resonators. A simple model to describe a semiconductor laser with optical feedback was introduced by Lang and Kobayashi [5]. The effect of TDAS on the Lang-Kobayashi model has already been investigated by Tronciu et al. [6]. That work was focused on stable continuous wave (cw) operation and how TDAS can disturb this cw-operation.

In this work we will investigate how time-delayed feedback methods can be successfully used to stabilize unstable steady states in such a semiconductor laser model. First, an extended Lang-Kobayashi-like model allowing undamped relaxation oscillations [7] will be introduced. Later the ETDAS feedback scheme will be applied to this model in order to suppress the relaxation oscillations and stabilize the fixed point leading to cw-operation. We calculate the domain of control in dependence on the control parameters and demonstrate our findings by a generic model of a fixed point [8], [9]. Furthermore, we support these results by data obtained from numerical simulations. Depending on initial conditions and control parameters, the system may show multistability. This leads to unwanted limit cycles and fixed points that evolve due to the presence of control.

This paper is organized as follows: In Section II we introduce a model of a semiconductor laser with passive dispersive feedback. This model allows for undamped relaxation oscillations for certain choices of the parameters. Furthermore, optical feedback by a Fabry-Perot resonator will be introduced into the model. In order to investigate the properties in the vicinity of the lasing fixed point, the model will be linearized in Section III. In Section IV the stability properties of the lasing fixed point without external feedback are investigated. The same is done in Section V in the presence of an external optical feedback. Results from numerical calculation are discussed in Section VI. The influence of various parameters will be shown, including the feedback strength, time delay, optical phase shift, and latency time. In Section VII a bandpass filter will be applied to the feedback signal. Again, numerical results show the impact on stability of the lasing fixed point. The manifold behavior of the system when deviating from the vicinity of the lasing fixed point will be briefly shown in Section VIII. Finally, we finish with a conclusion in Section IX.

II. The model

Semiconductor lasers with external optical feedback have been successfully described by the equations introduced by Lang and Kobayashi in 1980 [5]. In dimensionless form these include one equation for the complex electric field E and one equation for the carrier inversion n:

$$\frac{dE}{dt} = (1+\mathrm{i}\alpha)\, nE + Ke^{\mathrm{i}\varphi}E(t-\tau), \tag{1a}$$

$$\frac{dn}{dt} = \frac{1}{T}\left[I - n - (2n+1)\left|E\right|^2\right]. \tag{1b}$$

Here, E denotes the complex electric field, n the reduced carrier density, α the linewidth enhancement factor, K the feedback strength, φ the feedback phase, τ the delay due to external feedback, I the reduced injection current, and T the time scale separation. The variables I and n used in the Lang-Kobayashi model are transformed such that both are zero at the laser threshold.

In [7] Lang-Kobayashi-like equations are introduced which include a parameter $k(n)$ depending on internal passive dispersive feedback. The equations used there include a rate equation for the intensity. Instead of that, an equation

This work was supported by Deutsche Forschungsgemeinschaft in the framework of Sfb 555.

Institut für Theoretische Physik, Technische Universität Berlin, 10623 Berlin, Germany,schoell@physik.tu-berlin.de

for the electric field can be used, such that the equations read

$$\frac{dE}{dt} = \frac{T}{2}(1+\mathrm{i}\alpha)\,nE(t)+E_b(E(t)), \qquad (2a)$$

$$\frac{dn}{dt} = I-n(t)-[1+n(t)]\,k(n(t))\,|E(t)|^2. \qquad (2b)$$

The function $k(n)$, which models the internal dispersive feedback, is chosen as a Lorentzian, as introduced in [7]:

$$k(n) = k_0 + \frac{AW^2}{4\,(n-n_0)^2+W^2}, \qquad (3)$$

where A denotes the height, W the width, and n_0 the position of the resonance. The parameter k_0 is always chosen such that $k(0)=1$. A typical curve of $k(n)$ is shown in Fig. 1. Note that the chosen parameters correspond to the values used later in this work. In Eq. (2), the feedback

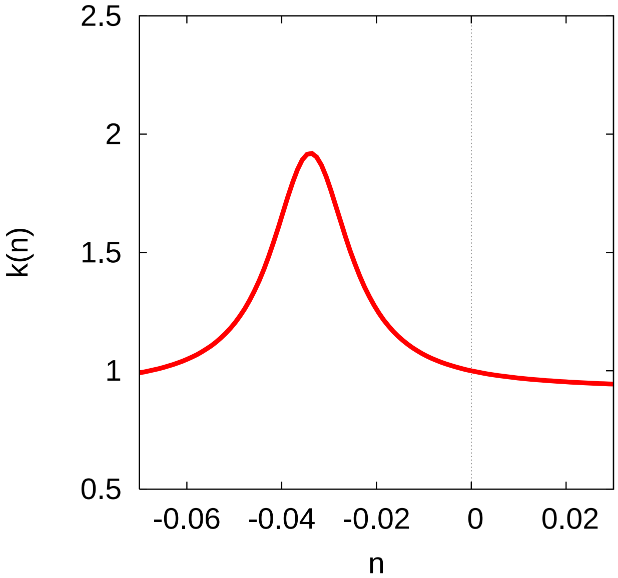

Fig. 1. Typical curve of the function $k(n)$ given by Eq. (3) used in the modified Lang-Kobayashi-like model described by Eq. (2). Parameters: $A=1$, $W=0.02$, and $n_0=-0.034$.

term $E_b(E(t))$ is written in a general form where the field that is fed back into the laser is not specified. We specify the feedback term, such that it models a Fabry-Perot resonator. As opposed to the original LK-model where a single external reflection is considered, an external Fabry-Perot (FP) resonator was considered here. The feedback term $E_b(E(t))$ can be written as follows, where we take only a single external reflection in the FP resonator into account:

$$E_b(E(t)) = Ke^{-i\varphi}\left[E(t-\delta)-e^{-\mathrm{i}\phi}E(t-\delta-\tau)\right], \qquad (4)$$

where the variables are named similar to Eq. (1). δ denotes a latency time due to the light traveling between laser and resonator and ϕ is the phase shift of the electric field in the FP resonator. This form of the feedback shows similarities a control scheme called *time-delay autosynchronisation* (TDAS), introduced by Pyragas [3]. This scheme is widely used due to the possibility of simple implementation in various applications. Furthermore, the scheme is noninvasive, meaning that the feedback signal vanishes, if the desired state of the system is reached. The effect of TDAS on unstable fixed points has already been investigated in a generic model by Hövel and Schöll [8].

Note that the latency time δ is correlated to the phase φ by the relation $\varphi=\Omega_0\delta$, where Ω_0 is the frequency of the emitted light. This is due to the fact that the amount of the phase shift of the light traveling between laser and FP cavity is related to the propagation time. The propagation time corresponds to the latency time δ. However, we let the two parameters φ and δ be independent, in order to keep the theory as general as possible.

The phase shift in the FP resonator, denoted by ϕ, has to be $2\pi m$, where m is an integer, in order to achieve noninvasive control. For $\phi\neq 0$ the feedback term would not vanish if $E(t-\delta)=E(t-\delta-\tau)$. Therefore $e^{-\mathrm{i}\phi}$ can be set to one.

Socolar et al. [4] introduced a generalization of the TDAS control scheme, where not only a state from the time $(t-\tau)$ is used to generate the feedback, but even early states are considered and weighted by a memory parameter. This extension is especially feasible for optical applications, where multiple reflections in optical resonators occur. This feedback scheme is known as the *extended time-delay autosynchronisation* (ETDAS).

If all external reflections in the previously considered FP-resonator are taken into account, the feedback term can be written in an ETDAS-like form including a memory parameter R:

$$\begin{aligned} E_b(E(t)) & \qquad (5) \\ &= Ke^{-i\varphi}\sum_{n=0}^{\infty}R^n\left[E(t-\delta-n\tau)-E(t-\delta-(n+1)\tau)\right] \\ &= Ke^{-i\varphi}\left[E(t-\delta)-E(t-\delta-\tau)\right]+RE_b(E(t-\tau)). \end{aligned}$$

Now that the model has been introduced, we investigate the stability of the lasing fixed point by a linearization around that point. Therefore, we will first consider the system without the feedback term.

III. Linearization around the lasing fixed point

The uncontrolled system has a fixed point at $(n=I, E=0)$. This fixed point is not of interest, because it describes a state which is not lasing, since the electric field is zero.

Another fixed point, which describes a lasing state is located at $(n=0, E=\sqrt{I}e^{\mathrm{i}\psi})$. Now, the phase of the electric field is arbitrarily fixed to $\psi=0$, such that $e^{\mathrm{i}\psi}=1$. This leads to symmetry breaking between the real and imaginary part of the electric field, meaning that the imaginary part, denoted by y in the following, is undetermined by the system's equations.

Using the abbreviations

$$E(t) = \sqrt{T}\left[\Omega_0+x(t)+\mathrm{i}y(t)\right], \qquad (6a)$$

$$\Omega_0 = \sqrt{\frac{I}{T}}, \qquad (6b)$$

$$\Gamma = \frac{1}{T}\left[1+I\left(1+\left.\frac{dk}{dn}\right|_{n=0}\right)\right], \qquad (6c)$$

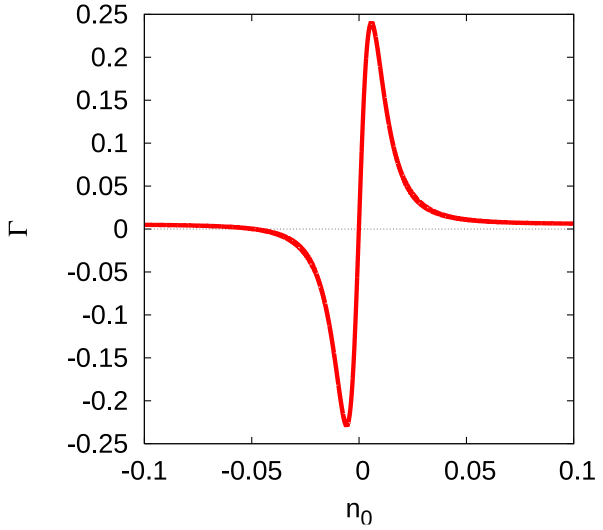

Fig. 2. Dependence of Γ on the choice of the parameter n_0 in the function $k(n)$ according to Eq. (6c)

with real-valued x and y, the fixed point is located at $(n = 0, x = 0, y = 0)$. A linearization around this point leads to the following system of equations:

$$\begin{pmatrix} \dot{n}(t) \\ \dot{x}(t) \\ \dot{y}(t) \end{pmatrix} = \begin{pmatrix} -2\Gamma & -4\Omega_0 & 0 \\ \Omega_0 & 0 & 0 \\ -\Omega_0\alpha & 0 & 0 \end{pmatrix} \begin{pmatrix} n(t) \\ x(t) \\ y(t) \end{pmatrix}. \qquad (7)$$

Note that an additional time scale transformation $t \longrightarrow (T/2)t$ was done to eliminate the parameter T from the equations. Also the function $k(n)$ is no longer present in the linearized equations. Instead, a parameter Γ was introduced that includes the derivative of $k(n)$. The relation between Γ and the parameter n_0 used in $k(n)$ according to Eq. (6c) is shown in Fig. 2.

The stability properties of the lasing fixed point can now be evaluated within this linearized model.

IV. Local stability of the uncontrolled system

In order to investigate the stability of the fixed point in the uncontrolled system, the characteristic equation can be derived. Therefore the determinant of the system's matrix has to be calculated, which results in the following equation:

$$\begin{aligned} 0 &= \det\left[\begin{pmatrix} -2\Gamma & -4\Omega_0 & 0 \\ \Omega_0 & 0 & 0 \\ -\Omega_0\alpha & 0 & 0 \end{pmatrix} - \Lambda\mathbf{Id}\right] && (8a) \\ &= \det\begin{pmatrix} -2\Gamma-\Lambda & -4\Omega_0 & 0 \\ \Omega_0 & -\Lambda & 0 \\ -\Omega_0\alpha & 0 & -\Lambda \end{pmatrix} && (8b) \\ &= \Lambda\left(\Lambda^2 + 2\Gamma\Lambda + 4\Omega_0^2\right), && (8c) \end{aligned}$$

where Λ denotes the eigenvalues of the system and $\mathbf{Id}$ is the identity matrix. This leads to solutions

$$\begin{aligned} \Lambda &= 0, && (9a) \\ \Lambda &= -\Gamma \pm \mathrm{i}\sqrt{4\Omega_0^2 - \Gamma^2}. && (9b) \end{aligned}$$

The solution $\Lambda = 0$ gives no information about the stability of the fixed point. This solution is only present due to the fact that y is undetermined by the system's equations. Therefore, only the second solution, given by Eq. (9b), is of interest.

Note that the imaginary part $\sqrt{4\Omega_0^2 - \Gamma^2}$, which corresponds to the frequency of the oscillation, leading to the focus characteristic of the fixed point, is only present if the condition $|2\Omega_0| > |\Gamma|$ is satisfied. Since $-\Gamma$ is the real part of the eigenvalue Λ, the focus is stable for any $\Gamma > 0$ and unstable otherwise.

Starting with an unstable focus ($\Gamma < 0$), we investigate whether or not the focus can be stabilized in the presence of the ETDAS control force.

V. Local stability of the controlled system

Adding ETDAS control to the linearized equations leads to the following system's equation in the linearization given by Eq. (7):

$$\begin{aligned} \begin{pmatrix} \dot{n}(t) \\ \dot{x}(t) \\ \dot{y}(t) \end{pmatrix} &= \begin{pmatrix} -2\Gamma & -4\Omega_0 & 0 \\ \Omega_0 & 0 & 0 \\ -\Omega_0\alpha & 0 & 0 \end{pmatrix} \begin{pmatrix} n(t) \\ x(t) \\ y(t) \end{pmatrix} \\ &\quad -K\begin{pmatrix} 0 & 0 & 0 \\ 0 & \cos\varphi & \sin\varphi \\ 0 & -\sin\varphi & \cos\varphi \end{pmatrix} \qquad (10) \\ &\quad \times \begin{pmatrix} \sum_{m=0}^{\infty} R^m \left[n(t-\delta-m\tau) - n(t-\delta-(m+1)\tau)\right] \\ \sum_{m=0}^{\infty} R^m \left[x(t-\delta-m\tau) - x(t-\delta-(m+1)\tau)\right] \\ \sum_{m=0}^{\infty} R^m \left[y(t-\delta-m\tau) - y(t-\delta-(m+1)\tau)\right] \end{pmatrix}. \end{aligned}$$

Using the an exponential ansatz $\exp(\Lambda t)$ for all three variables x, y, and n leads to a characteristic equation which reads

$$\begin{aligned} 0 &= (2\Gamma + \Lambda)\left[\left(Ke^{-\Lambda\delta}\frac{1-e^{-\Lambda\tau}}{1-Re^{-\Lambda\tau}}\right)^2 + \Lambda^2 \right. \\ &\qquad \left. + 2\Lambda Ke^{-\Lambda\delta}\frac{1-e^{-\Lambda\tau}}{1-Re^{-\Lambda\tau}}\cos\varphi\right] \\ &\quad + 4\Omega_0^2\left(\Lambda + Ke^{-\Lambda\delta}\frac{1-e^{-\Lambda\tau}}{1-Re^{-\Lambda\tau}}\cos\varphi\right. \\ &\qquad \left. - \alpha Ke^{-\Lambda\delta}\frac{1-e^{-\Lambda\tau}}{1-Re^{-\Lambda\tau}}\sin\varphi\right) \qquad (11) \end{aligned}$$

Before discussing the numerical results from this equation, some words regarding the used values for the parameters used in the model shall be inserted. In order to describe the physics as accurately as possible, the choice of the parameters may be essential. In [7] undamped relaxation oscillations were seen for the following values (These values are partially time scale transformed to match the equations used here.): $T = 500$, $I = 2$, $\alpha = 5$, $\Gamma = -0.25$, where T, I, α, and Γ are the time scale separation, the reduced injection current, the line width enhancement factor, and the damping parameter, respectively. Throughout our investigation we used the values given by Tab. I. Since $|\Gamma|$ needs to be smaller than $|2\Omega_0| = 0.12$ for the fixed point to have focus characteristics, a value of -0.25 would not have been possible. However, no control was possible in numerical

T	500
I	1.8
Ω_0	0.06
α	5
Γ	-0.01

TABLE I
VALUES USED FOR NUMERICS

simulations even for $\Gamma = -0.1$. Therefore, we chose a value of -0.01. The difference in I from the values given in [7] is just for the simplicity of Ω_0. For the simulation, an appropriate choice of the parameters A, W, and n_0 has to be made to match the value of $\Gamma = -0.01$ according to Eq. (6c). That can be achieved by the values given by Tab. II. Note that

A	1
W	0.02
n_0	≈ -0.034
k_0	≈ 0.920

TABLE II
VALUES USED FOR NUMERICS

the value of k_0 is determined by the other three parameters via the constraint $k(0) = 1$.

With the values given here, the domain of control will be investigated in the (K, τ)- and (K, R)-plane in the following.

VI. Numerical results

The stability of the lasing fixed point is given by Eq. (11). The parameter space consisting of K, τ, R, φ, and δ is five-dimensional for fixed Γ and Ω_0. To visualize the domain of control we consider projections onto two-dimensional parameter planes. We present results from a rootfinding algorithm. This algorithm calculates the roots of the characteristic equation numerically for different parameter sets, which allows for conclusions on stability achieved by the feedback.

In Fig. 3 the domain of control is shown in the (K, τ)-plane for different values of the phase φ. The color code denotes the largest real part of the eigenvalues and is therefore a measure of stability. Note that only values of $\mathrm{Re}(\Lambda) < 0$ are plotted, thus the shaded regions correspond to a stable lasing fixed point. It can be seen, that the domain of control shrinks for increase of the phase. Note that the minimum feedback is only slightly changed by increase of the phase. Instead, the regions of control are cut off from the right and top, leading to a decrease of the maximum feedback gain. Additionally, the secondary tongues at larger values of τ vanish by this cut-off. Also, the region of best stability, denoted by yellow/bright color code shrinks for increasing φ.

Figure 4 shows the domain of control in the (K, τ)-plane for values of φ in the range $[\pi, 2\pi]$, which corresponds to negative phases. The value of 2π corresponds to zero phase. Here, the domains of control are cut off from the upper left and right, leading to overall smaller regions of stability. The

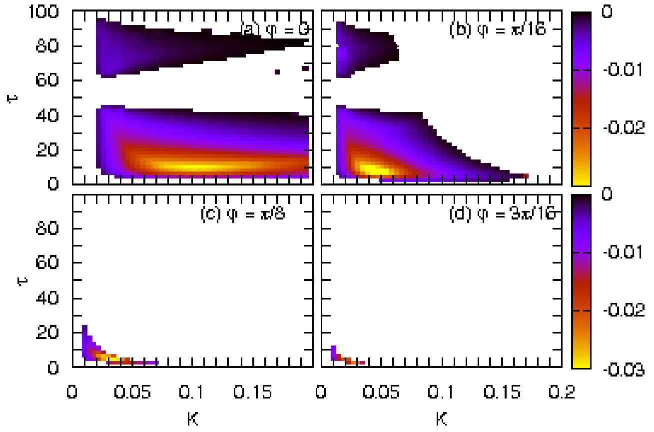

Fig. 3. Color online. Domain of control for the LK-like model according to Eq. (11)in the (K, τ)-plane for different values of φ. Results are from a rootfinding algorithm. The color code denotes the largest real part $\mathrm{Re}(\Lambda)$ of the eigenvalues Λ, only negative values are plotted. Parameters: $\Gamma = -0.01$, $\Omega_0 = 0.06$, $\alpha = 5$, and $R = 0.7$ as in [10]. Panels (a), (b), (c), and (d) correspond to $\varphi = 0$, $\pi/16$, $\pi/8$, and $3\pi/16$, respectively.

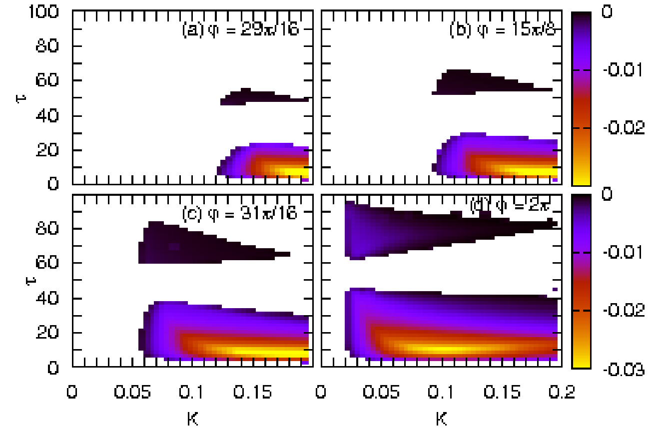

Fig. 4. Color online. Domain of control for the LK-like model in the (K, τ)-plane for different values of φ. Results are from a rootfinding algorithm. The color code denotes the largest real part $\mathrm{Re}(\Lambda)$ of the eigenvalues Λ, only negative values are plotted. Parameters: $\Gamma = -0.01$, $\Omega_0 = 0.06$, $\alpha = 5$, and $R = 0.7$. Panels (a), (b), (c), and (d) correspond to $\varphi = 29\pi/16$, $15\pi/8$, $31\pi/16$, and 2π, respectively.

tongues are also slightly distorted towards smaller values of τ. This is contrary to the generic model, where the tongues were only bent downwards for positive phase, and upwards for negative ones. This will have an effect on the domain of control in the (K, φ)-plane, which will be investigated at a later point. Additionally, in this picture, the regions of best stability, denoted by yellow/bright color, are shifted towards larger values of the feedback gain K.

As the effect of a nonzero phase was seen in the (K, τ)-plane, we will next investigate the role of the latency time.

In Fig. 5 the domain of control in the (K, τ)-plane is depicted for different values of the latency time δ and fixed $\varphi = 0$. Increasing the latency time, the domains of control are shrinked, but it can also be observed, that they are bent

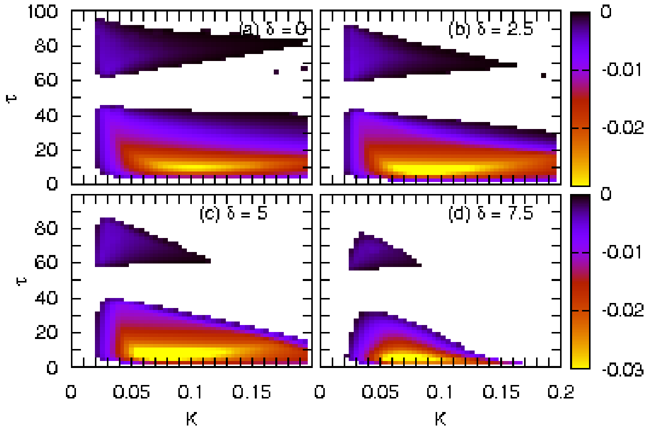

Fig. 5. Color online. Domain of control for the LK-like model in the (K, τ)-plane for different values of δ. Results are from a rootfinding algorithm. The color code denotes the largest real part $\mathrm{Re}(\Lambda)$ of the eigenvalues Λ, only negative values are plotted. Parameters: $\Gamma = -0.01$, $\Omega_0 = 0.06$, $\alpha = 5$, and $R = 0.7$. Panels (a), (b), (c), and (d) correspond to $\delta = 0$, 2.5, 5, and 7.5, respectively. Parameters: $\Gamma = -0.01$, $\Omega_0 = 0.06$, $\alpha = 5$, and $R = 0.7$.

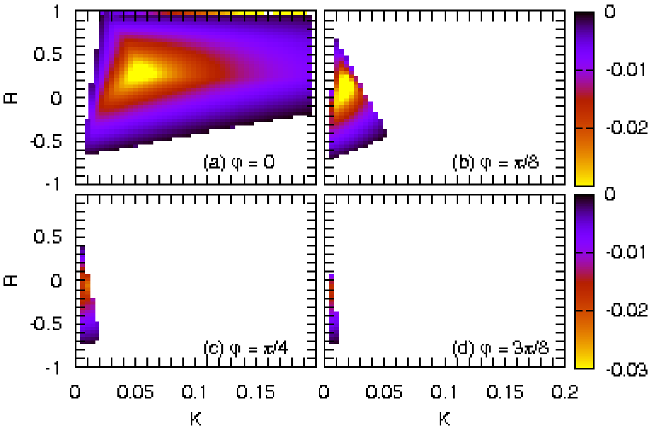

Fig. 6. Color online. Domain of control for the LK-like model in the (K, R)-plane for different values of φ. Results are from a rootfinding algorithm. The color code denotes the largest real part $\mathrm{Re}(\Lambda)$ of the eigenvalues Λ, only negative values are plotted. Parameters: $\Gamma = -0.01$, $\Omega_0 = 0.06$, $\alpha = 5$, and $\tau = 26$. Panels (a), (b), (c), and (d) correspond to $\varphi = 0$, $\pi/8$, $\pi/4$, and $3\pi/8$, respectively.

down towards smaller values of the time delay τ. Note that the regions of optimal stability, denoted by yellow/bright color, are only slightly affected by the change of the latency time. Overall, they are slightly smaller with larger δ.

All Figures shown here had a fixed value of the memory parameter $R = 0.7$. To investigate the dependence of the control on R, we show the domains of control in the (K, R)-plane.

Figure 6 shows the domain of control in the (K, R)-plane for different values of the phase φ and fixed time delay $\tau = 26$. This value of τ was chosen based on the results from the generic model considered in [8], [9]. There, it was shown that the optimal time delay is given by $\tau = \pi/\mathrm{Im}(\Lambda)$, where Λ was the eigenvalue of the uncontrolled system. In the LK model, the imaginary part of the eigenvalues in the uncontrolled system is given by Eq. (9b):

$$\mathrm{Im}(\Lambda) = \sqrt{4\Omega_0^2 - \Gamma^2}. \tag{12}$$

This leads to an optimal time delay according to $\tau_{opt} = \pi/\mathrm{Im}(\Lambda)$:

$$\tau_{opt} = \frac{\pi}{\sqrt{4\Omega_0^2 - \Gamma^2}}, \tag{13}$$

which leads to a value of $\tau_{opt} \approx 26$, since the parameters are $\Gamma = -0.01$ and $\Omega_0 = 0.06$.

Now, in Fig. 6, it can be seen, that the domain of control in the (K, R)-plane has maximum size for $\varphi = 0$ for this given time delay. For increasing phase, the domain of control is cut off from the upper right. Stability is then only achieved in a small region at small values of K and R. The region of optimal stability, denoted by yellow/bright color, keeps its position with increasing φ, but shrinks, since the whole region of control becomes smaller.

For the generic model as used in [8], it was shown, that for nonzero phase, stability through the control was enhanced, if

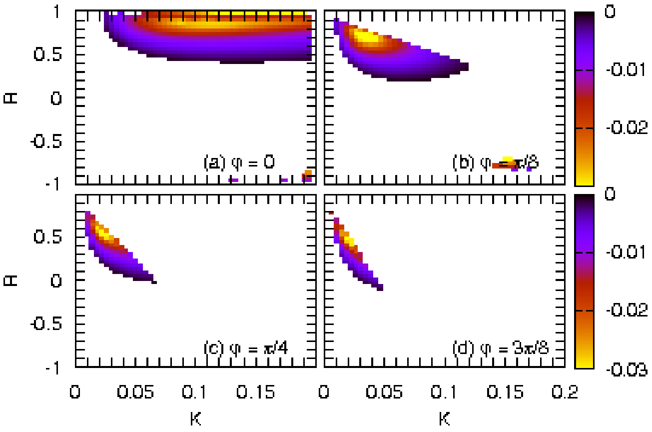

Fig. 7. Color online. Domain of control for the LK-like model in the (K, R)-plane for different values of φ. Results are from a rootfinding algorithm. The color code denotes the largest real part $\mathrm{Re}(\Lambda)$ of the eigenvalues Λ, only negative values are plotted. Parameters: $\Gamma = -0.01$, $\Omega_0 = 0.06$, $\alpha = 5$, and $\tau = 5$. Panels (a), (b), (c), and (d) correspond to $\varphi = 0$, $\pi/8$, $\pi/4$, and $3\pi/8$, respectively.

a delay time in the order of a fifth of the optimal time delay for vanishing phase was chosen. Therefore, we consider the domain of control in the (K, R)-plane for a value of $\tau = 5$ in Fig. 7. Here, the domain of control is already smaller in the case of $\varphi = 0$. Contrary to the generic model, the size of the region of stability is not enhanced here. Similar behavior as in Fig. 6 can be observed: The domain of control is cut off from the upper right for increasing phase. However, the domain is also shifted slightly towards smaller values of R and K, allowing for control with less feedback gain.

Same investigations as done here for nonzero phase, are made in the following for nonzero latency time δ and fixed $\varphi = 0$. In Fig. 8, the domain of control in the (K, R)-plane is shown for different values of the latency time and fixed

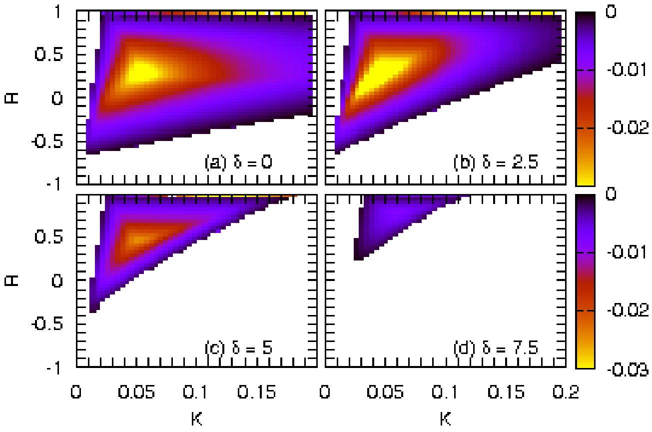

Fig. 8. Color online. Domain of control for the LK-like model in the (K, R)-plane for different values of δ. Results are from a rootfinding algorithm. The color code denotes the largest real part $\mathrm{Re}(\Lambda)$ of the eigenvalues Λ, only negative values are plotted. Parameters: $\Gamma = -0.01$, $\Omega_0 = 0.06$, $\alpha = 5$, and $\tau = 26$. Panels (a), (b), (c), and (d) correspond to $\delta = 0$, 2.5, 5, and 7.5, respectively.

$\tau = 26$. It can be observed, that the domain of control shrinks for increasing δ. The lower right boundary is shifted upwards. Therefore, control is only possible for large value of R with large δ. The minimum feedback gain is also increased, since the left boundary is shifted to the right. The regions of best stability, denoted by yellow/bright color vanish for increasing δ, leading to a loss of quality of the control.

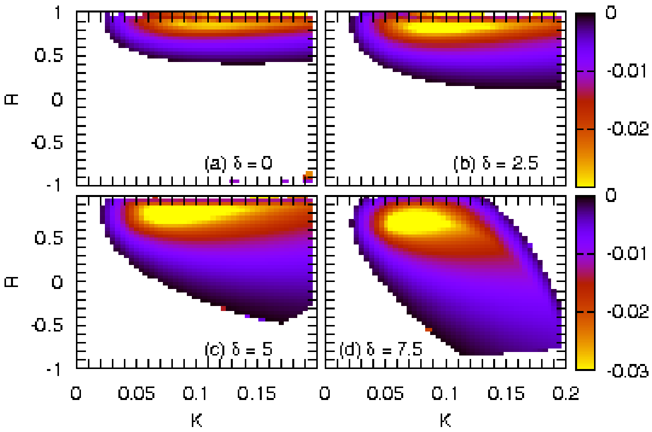

Fig. 9. Color online. Domain of control for the LK-like model in the (K, R)-plane for different values of δ. Results are from a rootfinding algorithm. The color code denotes the largest real part $\mathrm{Re}(\Lambda)$ of the eigenvalues Λ, only negative values are plotted. Parameters: $\Gamma = -0.01$, $\Omega_0 = 0.06$, $\alpha = 5$, and $\tau = 5$. Panels (a), (b), (c), and (d) correspond to $\delta = 0$, 2.5, 5, and 7.5, respectively.

There was also shown, that the stability is enhanced for a value of the time delay which is lower than the optimal value for zero latency time. Therefore, we depict the domain of control in the (K, R)-plane for a value of $\tau = 5$ and different values of δ in Fig. 9. The domain of control is smaller than in Fig. 8 for $\delta = 0$. However, the size of the domain of control is greatly enhanced for increasing the latency time. The region of stability is bent downwards towards lower values of the memory parameter R, allowing for control at a smaller value of the feedback gain for given R. The region of best stability is located at a large value of R for $\delta = 0$. This region also moves towards lower values of R and grows for increasing δ.

To investigate the dependence of the control on the choice of the phase φ further, we consider the (K, φ)-plane.

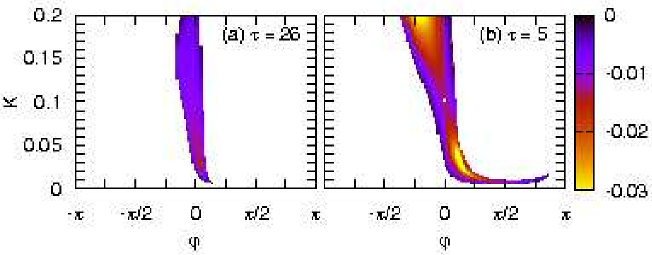

Fig. 10. Color online. Domain of control for the LK-like model in the (K, φ)-plane for different values of τ. Results are from a rootfinding algorithm. The color code denotes the largest real part $\mathrm{Re}(\Lambda)$ of the eigenvalues Λ, only negative values are plotted. Parameters: $\Gamma = -0.01$, $\Omega_0 = 0.06$, $\alpha = 5$, and $R = 0.7$. Panels (a) and (b) correspond to $\tau = 26$ and 5, respectively.

In Fig. 10 the domain of control is depicted in the (K, φ)-plane for two different values of the time delay with fixed $\delta = 0$. In panel (a), the time delay is chosen as 26, which is the optimal τ according to Eq. (13). Here, it can be seen, that the optimal phase is located at slightly positive values for small values of the feedback gain up to $K \approx 0.05$. Increasing K, the optimal phase changes its sign and is now located at small negative values of φ. For the case of $\tau = 5$, which is depicted in panel (b), stability is overall enhanced. The yellow/bright areas, denoting regions of best stability, are located at positive φ for small K up to $K \approx 0.1$. Control is possible even for a large value of φ exceeding $\pi/2$, if the feedback gain is tuned exactly to the small range of $K \approx 0.01$. For larger feedback gain with $K > 0.1$, the optimal value of φ is located at negative values. The region of best stability is located at large values of K around 0.2.

Since bandpass filters are widely used in optical systems, we will evaluate the effects on control in the LK model in the following Section.

VII. Bandpass Filtering of the Feedback Signal

A bandpass filter is widely used in experiments, as well as in theoretic treatments of the LK model, i.e., [11]. Therefore it is useful to include a corresponding term into the theory. The bandpass filter can be introduced by using the transfer function $T(\omega)$ in Fourier space. The transfer function of a band-pass filter modeled by a Lorentzian and acting on the electric field E can be written as

$$T(\omega) = \frac{1}{1 + \mathrm{i}\frac{\omega - \omega_0}{\gamma}}. \tag{14}$$

In Fourier space, the electric field filtered by the bandpass reads

$$\begin{aligned} \bar{E}(\omega) &= T(\omega)E(\omega) \\ &= \frac{1}{1+\mathrm{i}\frac{\omega-\omega_0}{\gamma}}E(\omega). \end{aligned} \tag{15}$$

Transforming back from Fourier space, this gives a differential equation for $\bar{E}(t)$:

$$\dot{\bar{E}}(t) = (\mathrm{i}\omega_0 - \gamma)\,\bar{E}(t) + \gamma E(t). \tag{16}$$

For the unfiltered system, the electric field complex variable $E(t)$ could be split into two variables $x(t)$ and $y(t)$ by using the identity $E(t) = \sqrt{T}[\Omega_0 + x(t) + \mathrm{i}y(t)]$. The filtered variable $\bar{E}(t)$ can also be split into some filtered counterparts $\bar{x}(t)$ and $\bar{y}(t)$. This leads to additional differential equations for the filtered variables $\bar{x}(t)$ and $\bar{y}(t)$:

$$\dot{\bar{x}}(t) = \gamma\,(x(t) - \bar{x}(t)) - \omega_0\bar{y}(t), \tag{17a}$$

$$\dot{\bar{y}}(t) = \gamma\,(y(t) - \bar{y}(t)) + \omega_0\bar{x}(t). \tag{17b}$$

Note that the same time scale transformation $t \to (T/2)t$ as in Eq. (7) has to be done here to keep all equations consistent. In order to keep the parameter T out of the equations, reduced parameters $\gamma \to 2\gamma/T$ and $\omega_0 \to 2\omega_0/T$ can be introduced. Then again, when using both the time scale transformation and the reduced set of γ and ω_0, no change has to be made to Eqs. (17).

In the following, we investigate the effects of these filtered variables $\bar{x}$ and $\bar{y}$. The system becomes five-dimensional with the following equations:

$$\begin{pmatrix} \dot{n}(t) \\ \dot{x}(t) \\ \dot{y}(t) \\ \dot{\bar{x}}(t) \\ \dot{\bar{y}}(t) \end{pmatrix} = \begin{pmatrix} -2\Gamma & -4\Omega_0 & 0 & 0 & 0 \\ \Omega_0 & 0 & 0 & 0 & 0 \\ -\Omega_0\alpha & 0 & 0 & 0 & 0 \\ 0 & \gamma & 0 & -\gamma & -\omega_0 \\ 0 & 0 & \gamma & \omega_0 & -\gamma \end{pmatrix} \times \begin{pmatrix} n(t) \\ x(t) \\ y(t) \\ \bar{x}(t) \\ \bar{y}(t) \end{pmatrix} - K \begin{pmatrix} 0 & 0 & 0 & 0 & 0 \\ 0 & 0 & 0 & \cos\varphi & \sin\varphi \\ 0 & 0 & 0 & -\sin\varphi & \cos\varphi \\ 0 & 0 & 0 & 0 & 0 \\ 0 & 0 & 0 & 0 & 0 \end{pmatrix} \mathbf{F}, \tag{18}$$

where the control force is given by the vector $\mathbf{F}$:

$$\mathbf{F} = \begin{pmatrix} \sum_{m=0}^{\infty} R^m\,[n(t-\delta-m\tau) - n(t-\delta-(m+1)\tau)] \\ \sum_{m=0}^{\infty} R^m\,[x(t-\delta-m\tau) - x(t-\delta-(m+1)\tau)] \\ \sum_{m=0}^{\infty} R^m\,[y(t-\delta-m\tau) - y(t-\delta-(m+1)\tau)] \\ \sum_{m=0}^{\infty} R^m\,[\bar{x}(t-\delta-m\tau) - \bar{x}(t-\delta-(m+1)\tau)] \\ \sum_{m=0}^{\infty} R^m\,[\bar{y}(t-\delta-m\tau) - \bar{y}(t-\delta-(m+1)\tau)] \end{pmatrix}.$$

For the sake of simplicity, we restrict ourselves to the case of $\varphi = 0$ and $\delta = 0$, which corresponds to the case of zero phase and no additional latency. The characteristic equation can then be derived by using an exponential ansatz $\exp(\Lambda t)$ for all five variables. The characteristic equation reads:

$$\begin{aligned} 0 &= 4\alpha\gamma\omega_0\Omega_0^2 K\frac{1-e^{-\Lambda\tau}}{1-Re^{-\Lambda\tau}} - \Lambda\omega_0^2\left(2\Gamma\Lambda + \Lambda^2 + 4\Omega_0^2\right) \\ &\quad - \left[\gamma K\frac{1-e^{-\Lambda\tau}}{1-Re^{-\Lambda\tau}} + \Lambda\,(\gamma+\Lambda)\right] \\ &\quad \times \left\{-\,(2\Gamma+\Lambda)\left[\gamma K\frac{1-e^{-\Lambda\tau}}{1-Re^{-\Lambda\tau}} + \Lambda\,(\gamma+\Lambda)\right] \right. \\ &\quad \left. -4\Omega_0^2\,(\gamma+\Lambda)\right\}. \end{aligned} \tag{19}$$

The eigenvalues Λ, which are the roots of the characteristic equation, were found by numerically solving this characteristic equation. The parameter space is five-dimensional, including K, τ, R, γ, and ω_0. Results are shown in projections onto different parameter planes in the following.

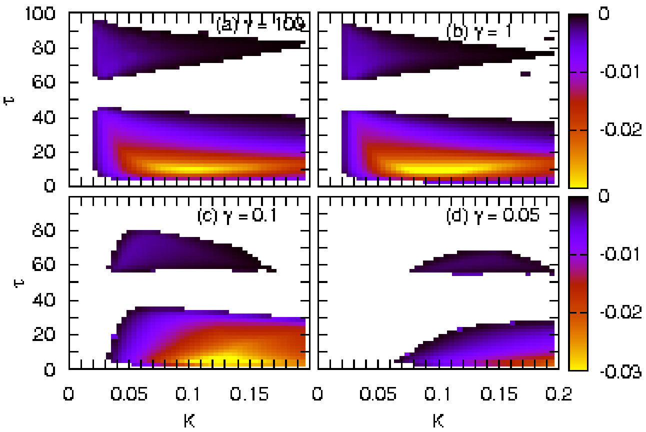

Fig. 11. Color online. Domain of control in the (K, τ)-plane according to Eq. (19) for different values of $\gamma = 100$, 1, 0.1, and 0.05 in panels (a), (b), (c), and (d), respectively. $\omega_0 = 0$ is fixed. Results are from a rootfinding algorithm. The color code denotes the largest real part $\mathrm{Re}(\Lambda)$ of the eigenvalues Λ, only negative values are plotted. Parameters: $\Gamma = -0.01$, $\Omega_0 = 0.06$, $\alpha = 5$, and $R = 0.7$. Panels (a), (b), (c), and (d) correspond to $\gamma = 100$, 1, 0.1, and 0.05, respectively.

In Fig. 11, the domain of control is shown in the (K, τ)-plane for different values of the filter width γ and fixed $\omega_0 = 0$. This corresponds to the case of the low-pass filter. The color code corresponds to the largest real part of the eigenvalues. For large values of γ, the picture is almost identical to the case of the unfiltered system shown in panel (a) of Fig. 3 on page 4. Decreasing the filter width to $\gamma = 1$ has only little effect on the shape of the domain of control, but the region of best stability, denoted by yellow/bright color, becomes larger. Decreasing γ further, the domain of control shrinks and is bent down slightly towards smaller values of τ. This suggests that the optimal τ changes, which will be investigated further in the (K, R)-plane.

Figure 12 depicts the domain of control in the (K, τ)-plane for different values of $\omega_0 = 0$, 0.001, 0.005, and 0.01 in panels (a), (b), (c), and (d), respectively. $\gamma = 0.1$ is fixed. The increase of ω_0 has only little effect on the stability. The tongues are narrower in τ direction and extended slightly in K direction. The shift of the optimal time delay will be studied in the following.

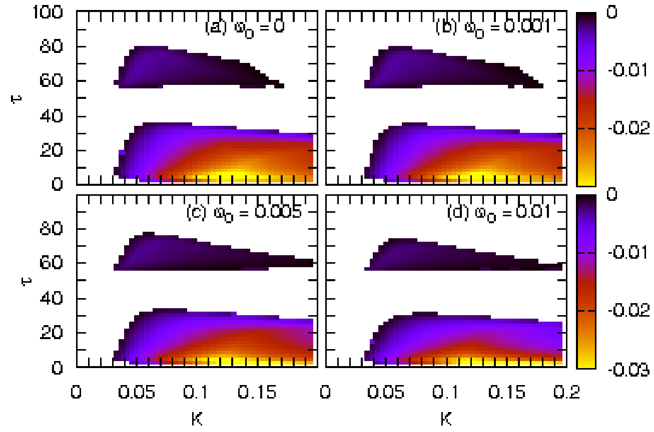

Fig. 12. Color online. Domain of control in the (K, τ)-plane according to Eq. (19) for different values of ω_0 with fixed $\gamma = 0.1$. Results are from a rootfinding algorithm. The color code denotes the largest real part $\mathrm{Re}(\Lambda)$ of the eigenvalues Λ, only negative values are plotted. Parameters: $\Gamma = -0.01$, $\Omega_0 = 0.06$, $\alpha = 5$, and $R = 0.7$. Panels (a), (b), (c), and (d) correspond to $\omega_0 = 0$, 0.001, 0.005, and 0.01, respectively.

Figures 13 and 14 show the domain of control in the (K, R)-plane for different values of the filter width γ and fixed $\omega_0 = 0$.

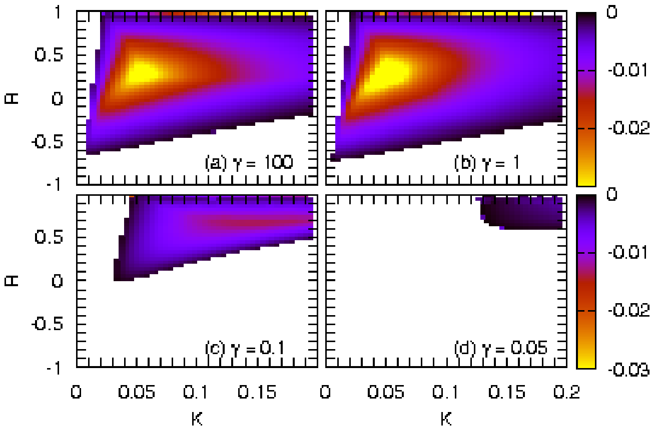

Fig. 13. Color online. Domain of control in the (K, R)-plane according to Eq. (19) for different values of γ with fixed $\omega_0 = 0$. Results are from a rootfinding algorithm. The color code denotes the largest real part $\mathrm{Re}(\Lambda)$ of the eigenvalues Λ, only negative values are plotted. Parameters: $\Gamma = -0.01$, $\Omega_0 = 0.06$, $\alpha = 5$, and $\tau = 26$. Panels (a), (b), (c), and (d) correspond to $\gamma = 100$, 1, 0.1, and 0.05, respectively.

In Fig. 13 the time delay is chosen as $\tau = 26$, which is the optimal time delay for the unfiltered system according to Eq. (13) on page 5. For the large value of the filter width $\gamma = 100$, the picture is almost identical to the unfiltered system, shown in panel (a) of Fig. 6. Decreasing the filter width to $\gamma = 1$ enlarges the domain of control slightly. Also, the region of best stability, denoted by yellow/bright color, is slightly larger. Decreasing γ to a value of 0.1, the domain of control shrinks and the quality of control is decreased, since the yellow/bright area vanishes. For $\gamma = 0.05$ the domain of control becomes very small. Control is only possible in for large value of K and R.

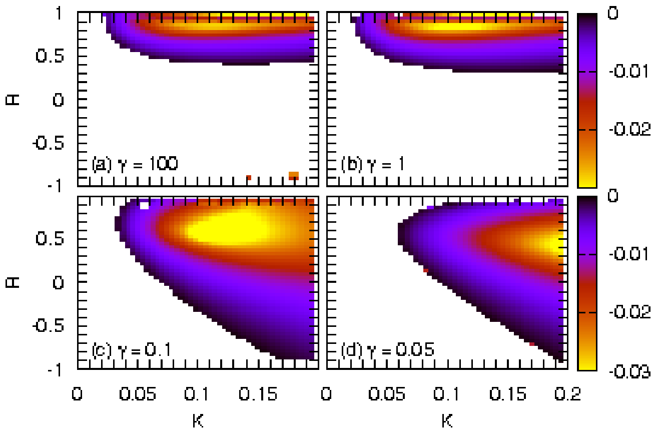

Fig. 14. Color online. Domain of control in the (K, R)-plane according to Eq. (19) for different values of γ with fixed $\omega_0 = 0$. Results are from a rootfinding algorithm. The color code denotes the largest real part $\mathrm{Re}(\Lambda)$ of the eigenvalues Λ, only negative values are plotted. Parameters: $\Gamma = -0.01$, $\Omega_0 = 0.06$, $\alpha = 5$, and $\tau = 5$. Panels (a), (b), (c), and (d) correspond to $\gamma = 100$, 1, 0.1, and 0.05, respectively.

The previous observations in the (K, τ)-plane suggested a shift of the optimal time delay towards smaller values. Therefore, Fig. 14 shows the domain of control in the (K, R)-plane similar to Fig. 13, but the time delay is chosen as $\tau = 5$ here. For $\gamma = 100$, the domain of control is much smaller than for the case of $\tau = 26$, control is only possible for large values of R. Decreasing the filter width to $\gamma = 1$ changes the domain only slightly by enlarging it in the R direction. For a value of $\gamma = 0.1$, the size of the domain of control is greatly enhanced, allowing for control at smaller values of R. The yellow/bright area, indicating best stability, is enlarged, leading to a wide choice of values for R and K. For $\gamma = 0.05$, the domain of control shrinks again and the yellow/bright area becomes smaller. Additionally, the domain of control is shifted towards larger values of K.

In the following the dependence of the domain of control on ω_0 is investigated. Therefore, Figs. 15 and 16 show the domain of control in the (K, R)-plane for fixed $\gamma = 0.1$ and different values of ω_0.

In Fig. 15, the time delay is chosen as $\tau = 26$. It can be seen, that an increase of ω_0 has only little effect on the domain of control. For $\omega_0 = 0.001$, the picture looks identical to the case of $\omega_0 = 0$. Increasing ω_0 further leads to domains of control that are shrinked in comparison with the case of $\omega_0 = 0$.

The domain of control in the (K, R)-plane for different values of ω_0 and the time delay chosen as $\tau = 5$ is depicted in Fig. 16. Again, the filter width is fixed to $\gamma = 0.1$. It can be seen that increasing ω_0 enhances both the size of the domain of control as well as the quality of the control. The lower left boundary of the domain is shifted to the left, allowing control for smaller values of the feedback gain K. Additionally, the yellow/bright areas become larger for increasing ω_0.

In all preceding considerations, the effect of ETDAS on

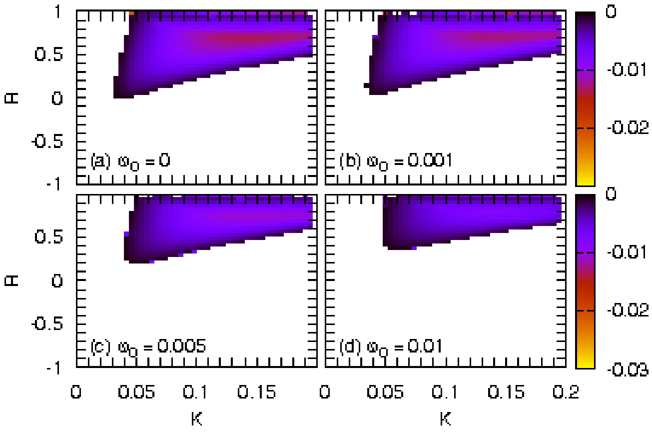

Fig. 15. Color online. Domain of control in the (K, R)-plane according to Eq. (19) for different values of ω_0 with fixed $\gamma = 0.1$. Results are from a rootfinding algorithm. The color code denotes the largest real part $\mathrm{Re}(\Lambda)$ of the eigenvalues Λ, only negative values are plotted. Parameters: $\Gamma = -0.01$, $\Omega_0 = 0.06$, $\alpha = 5$, and $\tau = 26$. Panels (a), (b), (c), and (d) correspond to $\omega_0 = 0$, 0.001, 0.005, and 0.01, respectively.

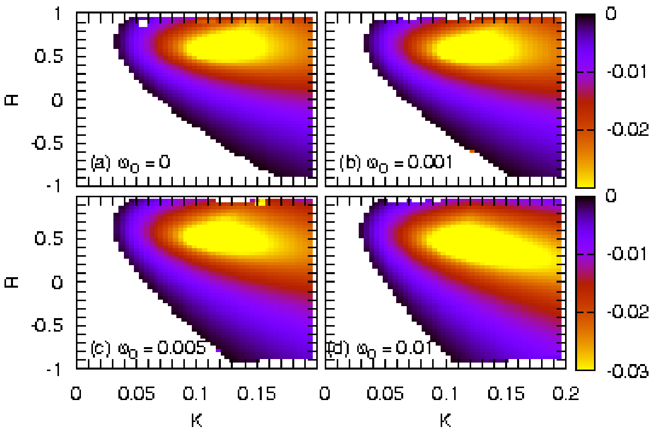

Fig. 16. Color online. Domain of control in the (K, R)-plane according to Eq. (19) for different values of ω_0 with fixed $\gamma = 0.1$. Results are from a rootfinding algorithm. The color code denotes the largest real part $\mathrm{Re}(\Lambda)$ of the eigenvalues Λ, only negative values are plotted. Parameters: $\Gamma = -0.01$, $\Omega_0 = 0.06$, $\alpha = 5$, and $\tau = 5$. Panels (a), (b), (c), and (d) correspond to $\omega_0 = 0$, 0.001, 0.005, and 0.01, respectively.

the stability of the lasing fixed point was investigated only locally, since the linearization around the fixed point was considered. Results from dynamical simulations of the full system, given by Eq. (2), with feedback according to Eq. (5), are shown in the following Section.

VIII. Delay-induced multistability

Since the laser model, described by Eq. (2), together with the feedback term Eq. (5), does not only have a fixed point which corresponds to the lasing state, further studies on the full dynamical systems are performed here.

Considering the model (2) without control, the system has a limit cycle in the $(|E|, n)$-plane, which corresponds to undamped relaxation oscillations. The radius of this limit cycle depends on the choice of the parameters. For the

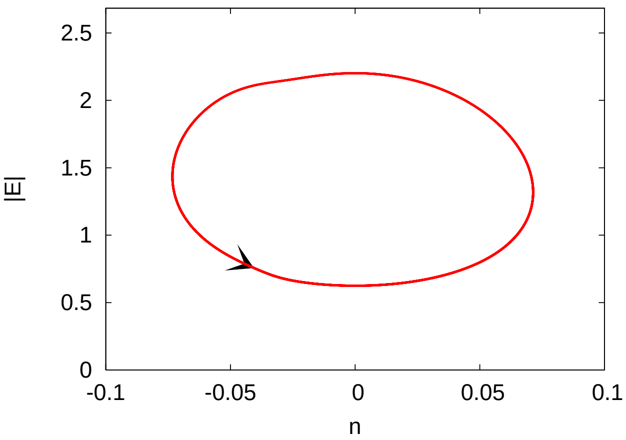

Fig. 17. Limit cycle of the undamped relaxation oscillations in the LK-like model given by Eq. (2) without feedback. Parameters: $T = 500$, $\alpha = 5$, $I = 1.8$, $A = 1$, $W = 0.02$, $n_0 = -0.034$, $k_0 = 0.920$. The arrow indicates the direction of the trajectory.

parameters used here, given by Tabs. I and II, the limit cycle is depicted in Fig. 17. The unstable fixed point is located at $(n = 0, |E| = 1.342)$ for this choice of parameters.

In an experiment, the case may be of interest, where the feedback is activated when the laser is operating at this limit cycle of relaxation oscillations. Therefore, we chose initial conditions on this limit cycle for numerical simulations. The electric field was chosen as $|E| = 0.727$, which corresponds to $x = -0.0913$ and $y = -0.00897$ with the parameters chosen according to Tabs. I and II. The reduced carrier density was chosen as $n = 0.0402$.

Depending on the feedback gain K and the time delay τ, the system shows diverse scenarios under the influence of feedback according to Eq. (5). Some trajectories of the system in the $(|E|, n)$-plane will be shown here.

In Fig. 18 trajectories of the system are depicted for fixed time delay $\tau = 26$ and different values of the feedback gain K. The memory parameter was fixed to $R = 0.7$. Limit cycles as well as chaotic attractors can be observed depending on the choice of K. In panel (a) the limit cycle of undamped relaxation oscillations is shown similar to Fig. 17, since the feedback gain is zero. Increasing the feedback gain to $K = 0.03$, a limit cycle of period 2 evolves. For a value of $K = 0.06$, chaotic behavior can be observed. Note that the trajectories are shown only for a limited span of time. At $K = 0.1$ a small limit cycle appears, but this limit cycle does not oscillate around the desired fixed point, which is located at $n = 0$. This limit cycle becomes smaller for $K = 0.12$ and grows again for $K = 0.15$. Note that for all these nonzero values of K the lasing fixed point at $n = 0$ is stable, but the system is not in the vicinity of the fixed point in order to get stabilized.

Figure 19 depicts trajectories in the $(|E|, n)$-plane for fixed feedback gain $K = 0.1$ and different values of the time delay τ. Again, manifold behavior of the system can be seen. In panel (a), i.e. $\tau = 0$, again, the limit cycle of

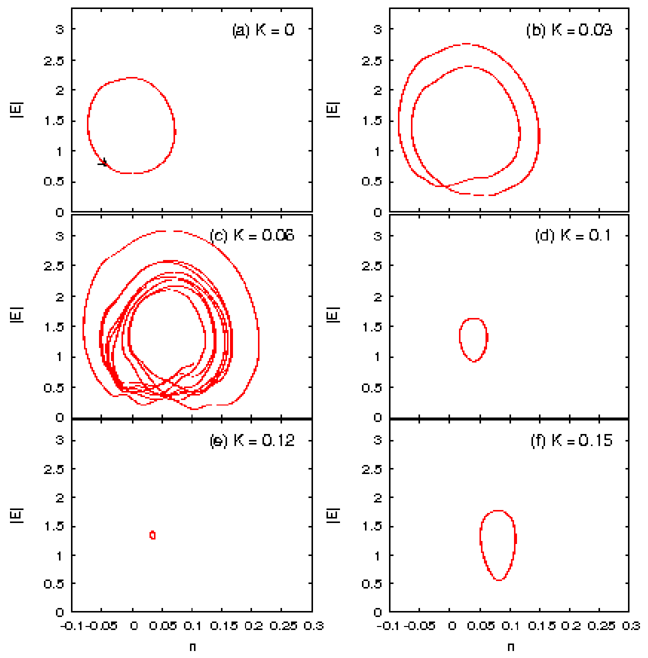

Fig. 18. Trajectories of the LK-like model with feedback for different values of the feedback gain K. Initial conditions are chosen on the limit cycle of relaxation oscillations. The time delay is fixed to $\tau = 26$. Other parameters: $R = 0.7$, $T = 500$, $\alpha = 5$, $I = 1.8$, $A = 1$, $W = 0.02$, $n_0 = -0.034$, $k_0 = 0.920$. Panels (a), (b), (c), (d), (e), and (f) correspond to $K = 0$, 0.03, 0.06, 0.1, 0.12, and 0.15, respectively. The rotational direction of the trajectories is the same as in panel (a) for all other panels.

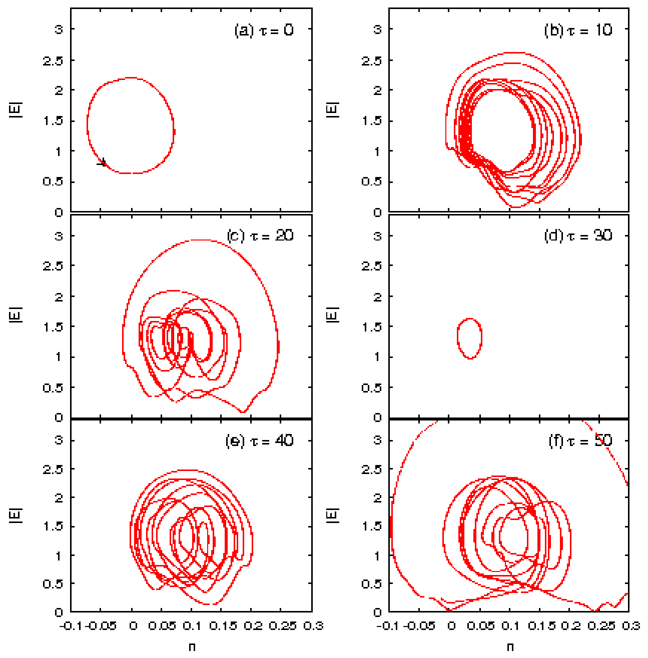

Fig. 19. Trajectories of the LK-like model with feedback for different values of the time delay τ. Initial conditions are chosen on the limit cycle of relaxation oscillations. The feedback gain is fixed to $K = 0.1$. Other parameters: $R = 0.7$, $T = 500$, $\alpha = 5$, $I = 1.8$, $A = 1$, $W = 0.02$, $n_0 = -0.034$, $k_0 = 0.920$. Panels (a), (b), (c), (d), (e), and (f) correspond to $\tau = 0$, 10, 20, 30, 40, and 50, respectively. The rotational direction of the trajectories is the same as in panel (a) for all other panels.

undamped relaxation oscillations is shown, since zero time delay corresponds to no control. Increasing the time delay, chaotic behavior can be seen for a wide range of the time delay, including $\tau = 10$, 20, 40, and 50. For $\tau = 30$ a limit cycle can be observed, that is similar to the one observed in panel (d) of Fig. 18. The radius may differ, since the time delay is not identical.

Looking more closely at a wider range of values of K and τ reveals even more possible attractors of the system with feedback. A detailed treatment is beyond the scope of this work. A bifurcation analysis, as well as an investigation of the dependence on the initial conditions, would provide more insight on this delay-induced behavior of the system and are subject of ongoing research.

IX. Conclusion

In conclusion, we have shown, that unwanted intensity pulsations in a semiconductor laser can be suppressed by time-delayed feedback methods. We have investigated that on a model of Lang-Kobayashi-type. Furthermore, we have shown that control can only be achieved in a vicinity of the lasing state. Depending on initial conditions, the system may show multistability for certain choices of the control parameters.

References

[1] *Handbook of Chaos Control*, edited by E. Schöll and H. G. Schuster (Wiley-VCH, Weinheim, 2007), second completely revised and enlarged edition.
[2] E. Ott, C. Grebogi, and J. A. Yorke, Phys. Rev. Lett. **64**, 1196 (1990).
[3] K. Pyragas, Phys. Lett. A **170**, 421 (1992).
[4] J. E. S. Socolar, D. W. Sukow, and D. J. Gauthier, Phys. Rev. E **50**, 3245 (1994).
[5] R. Lang and K. Kobayashi, IEEE J. Quantum Electron. **16**, 347 (1980).
[6] V. Z. Tronciu, H. J. Wünsche, M. Wolfrum, and M. Radziunas, Phys. Rev. E **73**, 046205 (2006).
[7] V. Z. Tronciu, H. J. Wünsche, J. Siebert, K. Schneider, and F. Henneberger, Opt. Commun. **182**, 221 (2000).
[8] P. Hövel and E. Schöll, Phys. Rev. E **72**, 046203 (2005).
[9] T. Dahms, P. Hövel, and E. Schöll, (2007), in preparation.
[10] S. Schikora, P. Hövel, H. J. Wünsche, E. Schöll, and F. Henneberger, Phys. Rev. Lett. **97**, 213902 (2006).
[11] H. Erzgräber, B. Krauskopf, D. Lenstra, A. P. A. Fischer, and G. Vemuri, Phys. Rev. E **73**, 055201 (2006).